

Article

Secondary Atomization of a Biodiesel Micro-Emulsion Fuel Droplet Colliding with a Heated Wall

Alexander E. Ashikhmin¹, Nikita A. Khomutov¹, Maxim V. Piskunov^{1,*}  and Vyacheslav A. Yanovsky²

¹ National Research Tomsk Polytechnic University, 30 Lenin Avenue, 634050 Tomsk, Russia; alashikhmin24@gmail.com (A.E.A.); nah7@tpu.ru (N.A.K.)

² National Research Tomsk State University, 36 Lenin Avenue, 634050 Tomsk, Russia; yavatpu@yandex.ru

* Correspondence: piskunovmv@tpu.ru; Tel.: +7-3822-701-777 (ext. 3465)

Received: 23 December 2019; Accepted: 13 January 2020; Published: 18 January 2020



Abstract: Using high-speed video recording, we establish the following regimes of hydrodynamic interaction of a biodiesel micro-emulsion fuel droplet with a heated wall: deposition (including drop spreading and receding), drop hydrodynamic breakup, and rebound. Collision regime maps are plotted using a set of dimensionless criteria: Weber number $We = 470\text{--}1260$, Ohnesorge number $Oh = 0.146\text{--}0.192$, and Reynolds number $Re = 25\text{--}198$. The scenarios of droplet hydrodynamic disintegration are studied for transient and film boiling. We also estimate the disintegration characteristics of a biodiesel micro-emulsion droplet (mean diameter of child droplets, their number, and evaporation surface area increase due to breakup). The study establishes the effect of water proportion on the micro-emulsion composition (8–16 vol.%), heating temperature (300–500 °C), droplet size (1.8–2.8 mm), droplet velocity (3–4 m/s), rheological properties of the examined compositions, and emulsifier concentration (10.45 vol.% and 20 vol.%) on the recorded characteristics. The results show that the initial liquid surface area can be increased 2–19 times. The paper analyzes ways to control the process. The hydrodynamic disintegration characteristics of a biodiesel micro-emulsion fuel droplet are compared using 2D and 3D recording.

Keywords: micro-emulsion fuel; biodiesel; heated wall; interaction; impact outcome; child droplets

1. Introduction

In many types of internal combustion engines operating on liquid fuel, droplets of an atomized fuel flow collide with a wall. Diesel engines often have quite a small combustion chamber, which makes the collisions of fuel droplets with the walls inevitable. Moreover, the trend of miniaturization is now common for engine design in general. All of this makes it especially important to understand and reliably predict the interaction of single fuel droplets with a heated surface [1]. Several practical matters are usually discussed [1–4] concerning different ways of droplet interaction with a wall in an engine. First, if droplets of atomized fuel are ignited without evaporating completely, the engine demonstrates lower combustion efficiency, while emitting unburnt hydrocarbons [2]. Second, the droplet-wall interaction may result in fuel sputtering, which in turn results in the formation of an air-fuel combustible mixture in the wall vicinity [3]. Third, in some engines, fuel evaporation may form gas-phase hot spots near the combustion chamber wall, which can lead to a destructive effect termed “super knock” [4]. Experimental research into the interaction of fuel droplets with a wall is also relevant because of the need to develop the existing mathematical models and create new ones to describe the processes in more detail.

The dynamics of carbohydrate fuel (heptane, decane, Jet A-1, diesel) interaction with a heated stainless steel wall in film evaporation regime was studied in [5]. The authors focused on analyzing the maximum droplet spreading diameter at various temperatures below the boiling point. The analysis shows that the maximum spreading diameter is significantly affected not only by the Weber number (We) and surface temperature (T_0), but also by the dynamic viscosity of fuel. The experimental data obtained was used to build an empiric model predicting the maximum spreading diameter of a fuel droplet on a heated surface and accounting for the temperature of the said surface.

Chen et al. [6] discovered that a diesel droplet does not interact with a heated surface in the same way as a droplet of water [7], *n*-heptane [8], or ethanol [9]. In particular, the duration of diesel droplet contact with a heated stainless steel surface does not depend on the impact angle or impact velocity, though it is 30% higher than for Rayleigh's free oscillation prediction. Moreover, Chen et al. established that the droplet disintegration criterion for diesel also differs from that of the other above liquids. The threshold We for a diesel droplet breakup is approximately 14.

In addition to the fuel viscosity affecting the interaction outcome, another important factor is the fuel component composition, which in its turn may affect the viscosity of the entire system. The interaction dynamics of a two-component fuel droplet and heated surface was experimentally studied by Kompinsky et al. [10]. A mixture of *n*-hexane and *n*-decane was used because these fuel types have a significant difference in boiling temperatures T_b . It was established that interaction regimes differ significantly for two-component and single-component fuel droplets. The study demonstrated the regimes typical of both two- and single-component droplets; however, some regimes were only typical of one of the considered droplet types. The research also showed that an increase in the velocity of droplet impact with the surface led to lower surface temperatures, thus specifying the interaction regime.

Another example of multi-component fuel droplet interaction with a heated wall is a series of experiments with biofuels—camelina-derived alternative jet fuels [11]. In this case, the fuel was a mix of Jet A-1 and camelina-derived biofuel. A typical Weber number (We) for droplets of this composition ranged from 28 to 886. A fuel droplet interacted with the stainless steel surface heated to a temperature of 25–350 °C. The study shows that the Leidenfrost point, i.e., the boundary between nucleate and film boiling, has a weak dependence on We . Temporal variations of normalized droplet contact diameter are studied at various surface temperatures. The paper identifies the spreading peculiarities for high- We droplets of the studied alternative fuel in the film boiling regime. In particular, the average spreading diameter was increasing. At the same time, in the cases of non-heated surface, film evaporation or nucleate boiling, it was slightly shrinking. It was established that the maximum spreading diameter at $We > 28$ increases with the surface temperature growth. Sen et al. [11] relate this effect to a decrease in surface tension and viscosity at growing T_0 when the T_0 is lower than the T_b of biofuel. In the case of $T_0 > T_b$, i.e., the film boiling regime, it is explained by the vapor flow generated between the wall and the droplet, which forces the spreading. Sen et al. [12] proposed the law of biofuel droplet spreading at high We , relating the spreading factor β and nondimensionalized time $\tau - \beta \sim \tau^{0.5}$. A good agreement was achieved between the experimentally obtained maximum spread factor β_{max} of a camelina biofuel droplet and the one theoretically predicted by the Ukiwe–Kwok model.

In terms of secondary atomization of isolated fuel droplets, the authors of [13–15] aimed at developing the empirical models to predict the size, velocity, and amount of secondary droplets resulting from the collision of parent drops with non-heated dry surfaces. In the case of homogeneous single-component fuel droplets, the studies are quite detailed on the wall impact regimes, mechanisms, and disintegration criteria accounting for the heat exchange mode [16], unlike multi-component droplets containing a dispersed phase of another liquid, i.e., emulsion [17,18], micro-emulsion [19–23], or nano-emulsion [24]. Moreover, the studied processes become even more complicated because the saturation temperatures of the liquids in emulsions, micro-emulsions, and nano-emulsions may differ drastically. This results in some unique aspects of droplet interaction with the heated wall (even those described in [25,26]) that should be studied in detail for each high-potential two- or multicomponent

fuel composition, just like it was done for urea water solution droplets [27]. Therefore, here we aim to study the interaction of multicomponent emulsion droplets with a heated surface with an emphasis on the secondary atomization as the most interesting regime for practical application. We are going to take into account the specific aspects outlined in this section concerning the outcomes of interaction between the droplets of conventional hydrocarbon fuels or alternative fuels, and their properties (surface tension, viscosity, and density).

The purpose of this study is to research the hydrodynamic regimes of interaction between biodiesel micro-emulsion fuel droplets and a heated wall, as well as to evaluate the integral characteristics of atomization by analyzing the number and size of the resulting child droplets.

2. Experimental

2.1. Experimental Set-Up

The experimental study of micro-emulsion droplets colliding with a horizontal heated wall was conducted on a typical setup schematically shown in Figure 1 and commonly used worldwide with slight modifications, e.g., [28,29]. The main elements are: heating plate (1.8 kW power, temperature setup accuracy ± 1 °C, operating temperature range 40–500 °C); metallic substrate (made of AlMg₆ alloy; roughness $R_a = 0.05$ – 0.12 μm measured with a Micro Measure 3D Station non-contact surface analyzer); droplet generator (micro-pump, syringe and hollow needle set with diameters of 0.33, 0.45, 0.6, 0.8, and 1.3 mm); lighting system with a diffusing panel; personal computer (PC) and two high-speed CMOS video cameras with a resolution of 768×480 px and frame rate of 8600 fps. Two cameras (Figure 1) allowed both planar (2D) and dimensional (3D) recording of the processes under study. A linear positioning module was used to vary the height of droplet generator placement above the substrate.

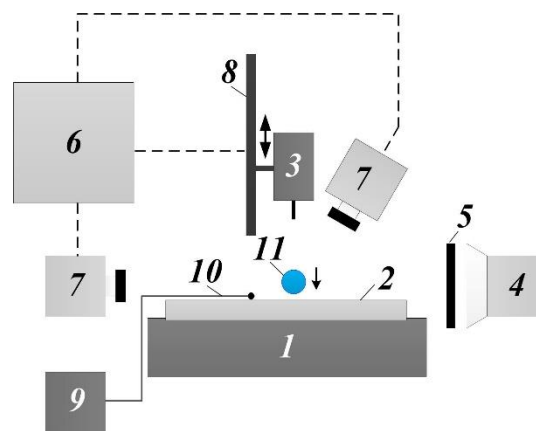


Figure 1. Scheme of the experimental setup: heating plate (1), substrate (2), droplet generator (3), LED spotlight (4), diffuser (5), PC (6), video camera (7), linear positioning module (8), data acquisition device (9), thermocouple (10), droplet (11).

The control setting of the heating plate was taken as the substrate surface temperature prior to the collision (T_0). The heating plate had a flat glass-ceramic surface and its area was 20 times larger than that of the substrate. Due to the natural roughness of the heating plate, the thermal contact between the plate and the substrate was imperfect. The contact heat-transfer resistance at the *heating plate–substrate* interface had no impact on the research findings, since the experiment was held in a steady state after heating and stabilizing temperature in the system (in particular, on the upper surface of the substrate) at the required level. This temperature was monitored via thermocouple readings. To increase the reliability of the temperature measurement, a half-spherical indentation 1 mm in diameter was made in the substrate upper surface to house an 80- μm thick thermocouple junction. The indentation was filled up with a heat sink compound to avoid an air gap at the *thermocouple junction–substrate* interface.

The thermocouple readings were recorded using a National Instruments 9219 converter connected to the PC. The accuracy of the substrate surface temperature T_0 readings was the same as the accuracy of the *thermocouple-converter-PC* measurement channel (± 10 °C or higher). The target values of T_0 will be given later.

2.2. Materials

The following materials were used to prepare the micro-emulsion fuel: diesel (EURO 3, type I-III (winter type) according to GOST R 52368–2005); fatty acid methyl ester of rapeseed oil (FAME of rapeseed oil, FAME of RO); biodiesel (B class, Vegakhim Ltd., Moscow, Russia); distilled water with the specific conductivity of no more than 5 $\mu\text{s}/\text{cm}$; Neonol AF 9-6 surfactant, polyethylene glycol ester (PEG-6) of isononylphenol, $\text{C}_9\text{H}_{19}\text{C}_6\text{H}_4\text{O}(\text{C}_2\text{H}_4\text{O})_6\text{H}$ (industrial grade, TU 2483-077-05766801-98, Nizhnekamskneftekhim, Nizhnekamsk, Russia); co-surfactant 2-ethylhexanol (industrial grade, GOST 26624-2016, Sibur-Khimprom, Perm, Russia). Table 1 contains diesel fuel properties and Table 2 gives the properties of fatty acid methyl ester of rapeseed oil.

Table 1. Diesel fuel properties.

Parameter	Value
Density at 25 °C (kg/m^3)	830
Kinematic viscosity ($\text{m}^2/\text{s}\cdot 10^6$) at:	
25 °C	2.780
40 °C	2.065
60 °C	1.515
80 °C	1.160
Closed cup flash point (°C)	60
Cloud point (°C)	−21

Table 2. Fatty acid methyl ester of rapeseed oil properties.

Parameter	Value
Density at 25 °C (kg/m^3)	870
Boiling point (°C)	300
Chilling point (°C)	−10
Acid number (mg KOH/g)	1
Ester number (mg KOH/g)	180.5

The micro-emulsion fuel samples were prepared by mixing the components in a glass vial according to the required volumetric fractions of the components.

To analyze the similarity criteria, we measured the density, viscosity, and surface tension of water-in-diesel (WiDME) and water-in-biodiesel (WiBDME) micro-emulsions (Figure 2). WiDME and WiBDME properties are given in Table 3. Table 4 contains the component composition of the resulting samples. The alternative fuel under study was stabilized with an emulsifier—A mixture of a surfactant (Neonol AF 9-6) and co-surfactant (2-ethylhexanol) with a volumetric mixture ratio of 9/1. The surface tension was measured using the ring method on a K6 tensiometer (KRUSS, Hamburg, Germany) at 22 °C. The density was calculated from the measured weight of the sample of the known volume. The viscosity was measured using an Ostwald-type capillary viscometer and a Brookfield DV3TLV viscometer (Brookfield Engineering Laboratories, Middleboro, MA, USA) with a thermostatically controlled cell. The droplet initial temperature was 25 °C.

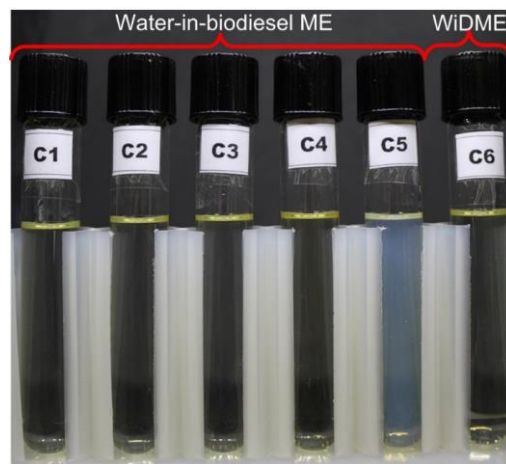


Figure 2. Water-in-diesel and water-in-biodiesel fuel compositions under study.

Table 3. Water-in-diesel and water-in-biodiesel micro-emulsion properties: surface tension (σ), density (ρ), kinematic viscosity (ν), and dynamic viscosity (μ).

Fuel Composition	σ (mN/m) at 25 °C	ρ (kg/m ³) at 25 °C	$\nu \cdot 10^6$ (mm ² /s) at 25 °C	$\mu \cdot 10^3$ (mPa·s) at 25 °C
C-1 *	29.7	902.42	39.89	36
C-2 *	30	902.75	51.84	46.8
C-3 *	29.9	910.36	46.14	42
C-4 *	29.8	892.4	31.33	27.96
C-5 *	30.9	892.11	32.01	28.56
C-6 **	29.03	893.13	45.16	40.33

Note: * WiBDME; ** WiDME.

Table 4. Component composition of the fuel under study.

Fuel Composition	Volumetric Ratio		Emulsifier Concentration (vol. %)
	D/FAME	D+FAME/Water	
C-1	90/10	80/20	20
C-2	70/30	80/20	20
C-3	50/50	80/20	20
C-4	90/10	90/10	20
C-5	50/50	80/20	10.45
C-6	100/0	80/20	20

2.3. Methods

The experiment determined the quantitative characteristics (Table 2) of hydrodynamic disintegration of micro-emulsion fuel droplets interacting with a heated wall: d_s is the arithmetical mean diameter of child droplets generated by hydrodynamic disintegration (also known as d_{10}); N is the number of child droplets; S_1 is the total evaporation surface area of child droplets. The latter characteristic is determined as the area of a single fragment with the diameter d_s further multiplied by N (see the calculation method for d_s and N below). In addition, the initial surface area S_0 of a parent droplet was calculated as the area of a sphere of the known diameter D_0 .

The parameter d_s was calculated in the Mathematica software package. A custom program was developed to analyze the resulting disintegration of fuel micro-emulsion droplets (i.e., the mean diameter of the generated fragments). A binarization threshold was set individually for each processed image. Then the program identified the elements and calculated their dimensions in pixels. The software subtracted the background and rejected the elements adjacent to the image border. Since the substrate had a mirror-like finish, the reflection of fragments was erased from the image during the frame processing. The designed technique is discussed in detail in [30]. N is a parameter calculated by: (1) determining the volume of a single child droplet with the mean diameter d_s ; (2) determining the

initial volume of a droplet with the diameter D_0 . Next, the initial volume of a droplet with the diameter D_0 was divided by the volume of a fragment with the diameter d_s . The resulting value was an estimate of N . There are several papers, for example [31], describing the evaluation of the number of fragments generated from a droplet breakup after heating or collision with a wall, another droplet or a group of droplets (aerosol). The parameter S_1 was computed by

The properties of micro-emulsions from Table 1 were used to calculate the Weber number (We) [16], Reynolds number (Re) [16], and Ohnesorge number (Oh) [16] to account for the inertial forces, viscosity, and surface tension:

$$We = \rho D_0 U_0^2 \sigma^{-1} \quad (1)$$

$$Re = D_0 U_0 \nu^{-1} \quad (2)$$

$$Oh = \mu(\sigma \rho D_0)^{-0.5} \quad (3)$$

where D_0 is the diameter of a droplet prior to its collision with the substrate, mm; U_0 is the velocity of a droplet prior to its collision with the substrate, m/s; ν is kinematic viscosity, m^2/s ; ρ is density, kg/m^3 ; σ is surface tension, N/m; and μ is dynamic viscosity, Pa·s.

In the experiments, the parameter D_0 was 1.8–2.7 mm and the parameter U_0 was ~3 m/s and ~4 m/s. The substrate surface temperature T_0 varied in the range of 300–500 °C. At this temperature, droplets of the micro-emulsion fuel colliding with the substrate consistently underwent hydrodynamic disintegration for every U_0 and D_0 under study. At a temperature lower than 300 °C, the disintegration was inconsistent; at even lower temperatures, hydrodynamic disintegration was replaced by droplet deposition on the surface.

To study the hydrodynamic interaction regimes of WiBDME and WiDME droplets (see Section 3.1 for the results), we conducted experiments for D_0 ranging from 1.75 mm to 3 mm and U_0 from 0.9 m/s to 3.1 m/s. The regime was determined after 3 to 5 experiments.

The quantitative characteristics were derived from the results of 3 to 7 experiments. The systematic error of the measurement depends on the focal depth of the lens (when counting the atomized droplets) and settings of the measuring system for d_s (processed in Phantom Camera Control software on the basis of the scale coefficient calculated from the known object size in the recording area), and did not exceed 10% in both cases.

3. Results and Discussion

There are a number of the factors that influence the WiDME and WiBDME droplet impact onto a heated wall. Among them are the characteristics of an injector, the angle of injection, the drop impingement angle, the fuel injection pressure (common rail pressure), impact drop size and velocity, rheological properties of fuel micro-emulsions and bio-additive, emulsifier and water concentrations in fuel micro-emulsions, etc. In the study, we will discuss in detail the effects of the three last factors. However, first we have established the possible regimes of WiDME and WiBDME droplet interaction.

3.1. Hydrodynamic Interaction Regimes of WiDME and WiBDME Droplets

The analysis of the experimental results, like in [32], established that there are three possible regimes of WiDME and WiBDME droplet interaction. Figure 3 shows the images corresponding to the established regimes: (a) drop deposition (including drop spreading and receding), (b) drop hydrodynamic breakup, (c) drop rebound. This indicates that the bio-additive to the fuel micro-emulsion had no significant effect on the hydrodynamic interaction between the droplets and heated surface.

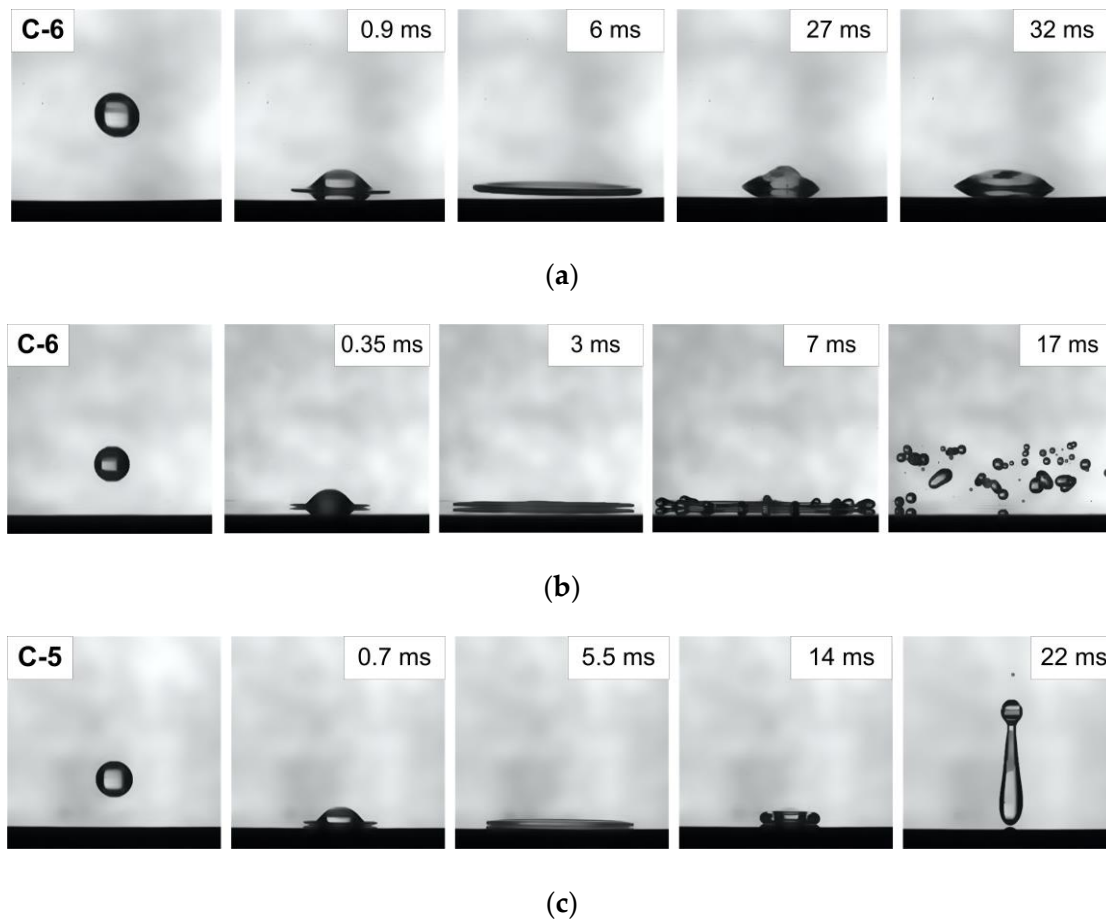


Figure 3. WiDME and WiBDME drop collision with a heated surface within different hydrodynamic regimes: (a) drop deposition (including drop spreading and receding), $T_0 = 225\text{ °C}$, $D_0 \approx 3\text{ mm}$, $U_0 \approx 1.72\text{ m/s}$, (b) drop hydrodynamic breakup, $T_0 = 320\text{ °C}$, $D_0 \approx 2.7\text{ mm}$, $U_0 \approx 2.69\text{ m/s}$, (c) drop rebound, $T_0 = 330\text{ °C}$, $D_0 \approx 3\text{ mm}$, $U_0 \approx 1.72\text{ m/s}$.

The effect of inertial forces, viscosity, and surface tension results in different outcomes of the impact characterized by specific thermodynamic processes. In the case of drop deposition regime (Figure 3a), just like for distilled water [29], a micro-emulsion fuel droplet is wetting the surface during its whole lifetime and does not rebound after the impact. After the impact, the droplet evaporation is accelerated under the effect of convection or bubble boiling, depending on T_0 . For the distilled water, the authors of [29] describe drop dancing as a transient regime between drop deposition and drop rebound. In the experiments with WiDME and WiBDME droplets, this regime was not observed, most likely, because their viscosity is higher than that of water. No transient boiling was identified by video-recording in the micro-emulsion under study.

The drop rebound regime (Figure 3c) is characterized by high surface heating temperature T_0 . After spreading and receding, the drop rebounds. The reason for this behavior is a vapor layer between the substrate surface and the droplet. Film boiling during droplet interaction is described in [33,34].

In terms of practical secondary atomization, the hydrodynamic breakup regime (Figure 3b) is of the highest interest. This regime produces a lot of secondary droplets, also known as child droplets. In real internal combustion engines, this regime will accelerate the ignition of the air-fuel mixture. The numerical characteristics of this interaction regime will be presented further. The transition boundary between the regime of hydrodynamic breakup of micro-emulsion fuel droplets and their rebound for various D_0 and U_0 is shown in Figure 4 and is given by $Re = -1466.7Oh + 349.33$. More details on this transition and the analysis of the regime map in Figure 4 can be found in [32].

When generalizing the results using Re and Oh , we attempt to determine the balance of inertial forces, viscosity, and surface tension that leads to a transition from one droplet-wall interaction regime to another. The overall shape of the transition boundary in Figure 4 demonstrates the possible transition to extensive atomization of droplets with high viscosity to surface tension ratio, even at relatively low Re (below 100). For actual advancement of the technology, this result can be used to rationalize that lower pressures are sufficient for fuel injection (with lower velocity and Re). The experiments showed that the higher the liquid viscosity, the faster the child droplets take spherical shape. It requires higher aerodynamic force to disrupt spherical drops than elliptical or disk-shape ones [35]. It decreases the probability of recurrent breakup, i.e., high-viscosity liquid can be atomized by an injection nozzle (primary) and by wall impact (secondary), but all the following stages will not provide many child droplets. In general, high-viscosity liquid is characterized by the lower amount and larger dimensions of child droplets.

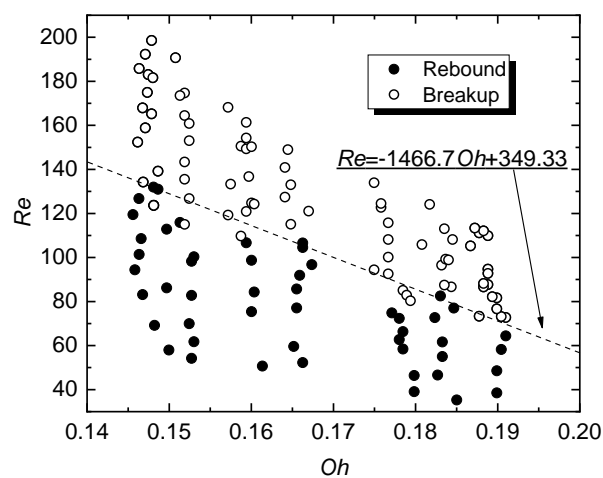


Figure 4. Hydrodynamic interaction regime map of a WiDME droplet and a heated surface as a function $Re(Oh)$, $T_0 = 320\text{ }^\circ\text{C}$.

Figure 5 shows experimentally recorded frames of the hydrodynamic breakup of WiDME and WiBDME drops. Similar interaction types are thoroughly studied in a number of papers, in particular [10,11,16,25], for droplets of fuel and hydrocarbon two-component mixtures, as well as biofuel compositions. In this study, we present the data on the hydrodynamic breakup of micro-emulsion fuel droplets interacting with a heated horizontal wall.

Using the terms from [16] we recorded the following interaction stages in our experiments: stick, prompt splash, corona splash, spread, fingering, finger breakup, and rebound. Figure 5a shows a prompt splash mixed with a finger breakup when a part of the liquid sticks to the surface in a transient boiling regime creating localized areas of heat supply to the liquid. The process is characterized by the intense phase transition, chemical reactions, and consecutive significant fuming. Fingering followed by finger breakup was also recorded separately (Figure 5b). However, the central area of the drop lamella, excluding the rim and the resulting fingers, can be disrupted by film boiling [16]. Notably, a part of child droplets generated from the disrupted central area visually travel upward from the substrate, unlike the finger breakup when they travel along the substrate surface. It is clearly demonstrated in Figure 5b. A corona splash was also recorded (Figure 5c).

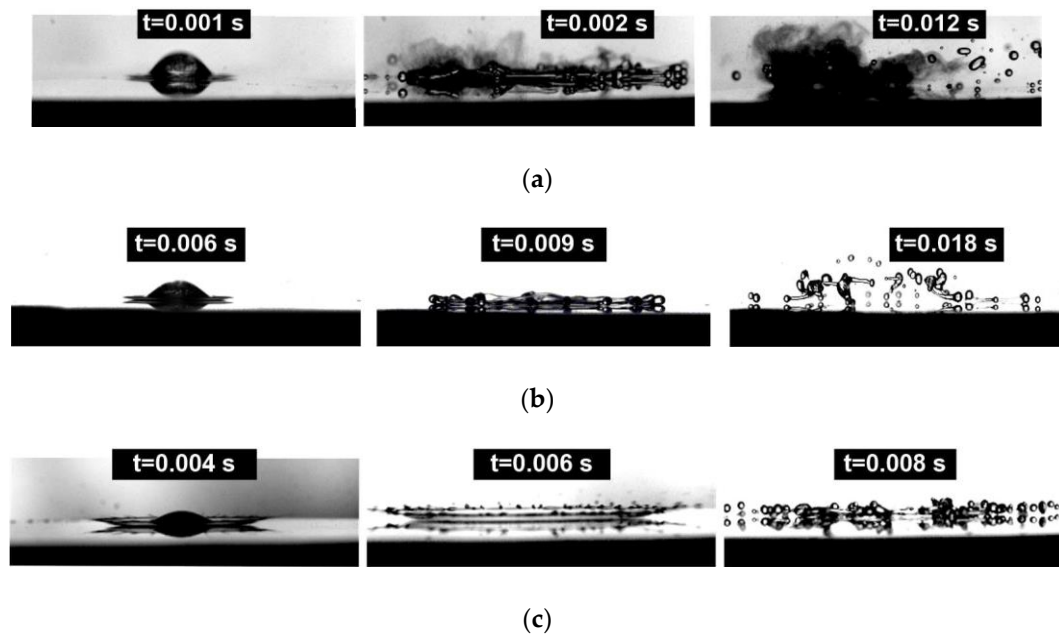


Figure 5. Types of hydrodynamic breakup of WiDME and WiBDME drops: (a) breakup by transient boiling with fuming, C-1, $T_0 = 300$ °C, $D_0 = 2.3$ mm, $U_0 = 3$ m/s; (b) prompt splash and film boiling breakup, C-3, $T_0 = 300$ °C, $D_0 = 2.25$ mm, $U_0 = 3$ m/s; (c) corona splash breakup, C-5, $T_0 = 500$ °C, $D_0 = 2.25$ mm, $U_0 = 3$ m/s.

Recording from above (three-dimensional recording) allows a more detailed analysis of spread, prompt splash, and finger breakup, as well as disruption in the central area of the drop lamella with cells, filaments, and fingers (Figure 6) forming in the transient boiling (Figure 6b) and film boiling (Figure 6a) regimes.

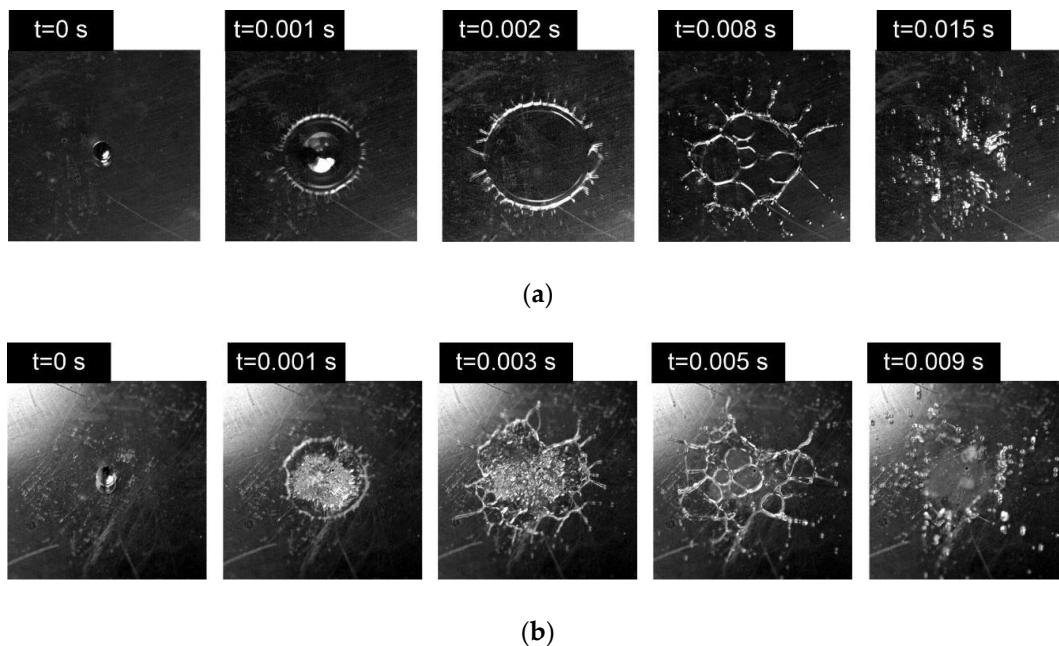


Figure 6. WiBDME drop hydrodynamic breakup regimes: (a) film boiling breakup, C-1, $T_0 = 500$ °C, $D_0 = 2.9$ mm, $U_0 = 3$ m/s; (b) transient boiling breakup, C-1, $T_0 = 300$ °C, $D_0 = 2.9$ mm, $U_0 = 3$ m/s.

In the study, transient boiling means that the lamella partly touches the heated surface, enhancing the intense vaporization with a formation of small vapor bubbles (Figure 6b). Generally, the breakup

occurs under such vaporization. As a comparison, the hydrodynamic breakup under the film boiling is depicted in Figure 6a.

3.2. Effect of Impact Velocity

When estimating the quantitative parameters of the hydrodynamic breakup in a two-dimensional regime, we established the contribution of the variation in the droplet velocity U_0 before reaching the substrate surface. Figure 7a shows the variation of d_s/D_0 (its decrease indicates a decrease in d_s , the mean child droplet diameter) depending on We and the substrate surface temperature T_0 . The analysis of the results from Figure 7a brings us to the following conclusion:

- (1) For the same T_0 and U_0 and growing We only due to an increase in D_0 , the mean diameter of child droplets decreases moderately, in some cases by 50%. In general, for the current experimental conditions, a larger initial drop diameter provides finer child droplets.
- (2) T_0 growth does not provide finer dispersion.
- (3) With increasing We , the difference in d_s/D_0 for various T_0 approaches a certain minimum.
- (4) An increase in U_0 provides a finer dispersion of micro-emulsion fuel drops; in other words, a considerable growth of inertial forces (i.e., 2–2.5 times higher We) decreases d_s (up to 1.5–2.5 times in our conditions).

Figure 7b shows how the interaction velocity of fuel micro-emulsion drops affects the number of child droplets depending on T_0 . The analysis of the results from Figure 7b revealed a number of features:

- (1) A minor increase in U_0 leads to a several-fold increase in N . D_0 also has a noticeable impact. Its growth causes N to increase, i.e., a micro-emulsion droplet of a larger initial volume disperses into more fragments of smaller dimensions (Figure 7a).
- (2) T_0 growth has a moderate effect on N . However, an important exception is observed at $T_0 = 500$ °C. For almost every case from Figure 6b, there is a relative increase in N at this temperature. We link this to an intense film boiling breakup (Figures 5b and 6a), which is typical of this T_0 .

The resulting conclusion is as follows: film boiling during the hydrodynamic breakup provides finer dispersion of a drop (Figure 6a), while forming more child droplets (Figure 7b).

S_1/S_0 is an integral parameter evaluating the effect of drop impact velocity variation on the hydrodynamic breakup characteristics. A minor increase in the impact velocity provides a consistent growth of the evaporation surface area (Figure 7c). The most prominent increase in the evaporation surface area is observed at the minimum examined temperature $T_0 = 300$ °C. An increase in the substrate surface temperature has an overall negative effect on the evaporation surface area increase, although no major loss of the parameter occurs. Since it is a calculated parameter, the reasons for S_1/S_0 increase are similar to those of the results in Figure 7a,b.

The experimental results from Figure 7 demonstrate the dominant effect of drop impact velocity on child droplet characteristics for a wide range of We and wall temperature variation. The analysis of the recorded images and data [35] indicates that an increase in the droplet velocity increases the inertia and intensifies the surface deformation of a moving droplet from a spherical shape. This extends the interaction area with the wall, which increases the number of child droplets and reduces their size.

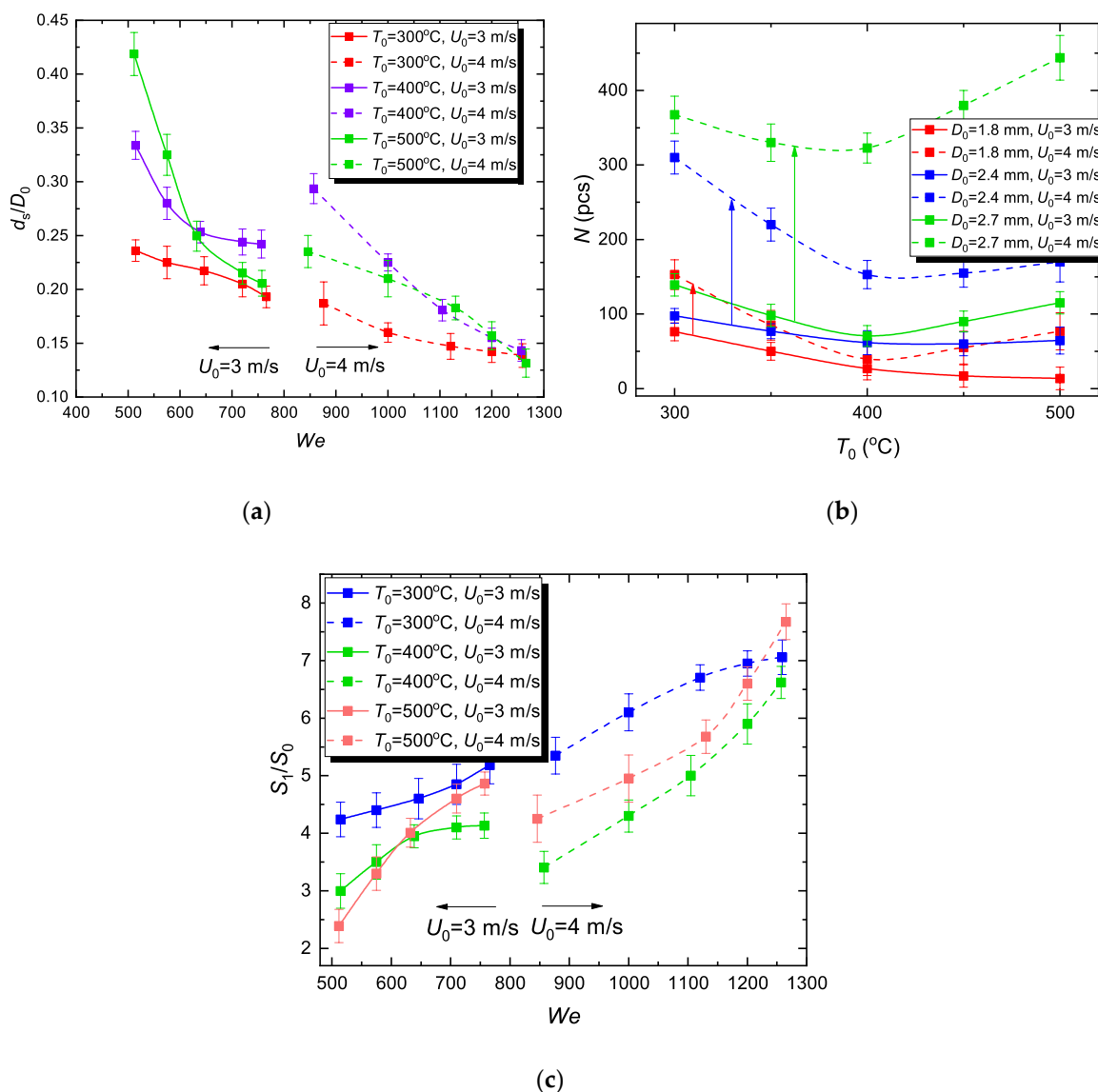


Figure 7. Effect of WiDME (C-6) drop interaction velocity on variation of the mean diameter of child droplets generated by hydrodynamic breakup (a), their number (b), and evaporation surface area (c) at various surface temperatures.

3.3. Effect of Rheological Properties of Fuel Micro-Emulsions and Bio-Additive

We estimated how the FAME of rapeseed oil bio-additive affects the mean diameter of child droplets generated by the hydrodynamic breakup (Figure 8a). It was established that the additional component provides a decrease in d_s . Also, the minimum considered amount of this component ($D/RO = 90/10$) leads to the most substantial decrease in the mean child droplet diameter. A further increase in the biodiesel proportion increases d_s/D_0 . This result can be explained by different kinematic viscosity of the examined fuel compositions. In particular, sample C-1 has the lowest viscosity and the smallest mean diameter of child droplets (Figure 8a). In other words, lower viscosity gives finer droplets. This pattern was observed throughout the range of the heating temperatures under study.

Moreover, the droplet of C-1 with the lowest viscosity breaks up into the largest amount of child droplets as well (Figure 8b). Interestingly, adding the lowest examined amount of rapeseed oil caused a *several-fold* (from ~ 100 up to >1000) increase in the number of child droplets under the same experimental conditions. A further increase in the biodiesel fraction has a moderate effect on N (increasing it 2–5 times). Finally, it was no surprise that the estimated increase in the evaporation

surface area due to hydrodynamic breakup was maximum for the C-1 composition at $T_0 = 400\text{ }^\circ\text{C}$ (Figure 8c). The initial drop surface area was exceeded by more than 10 times.

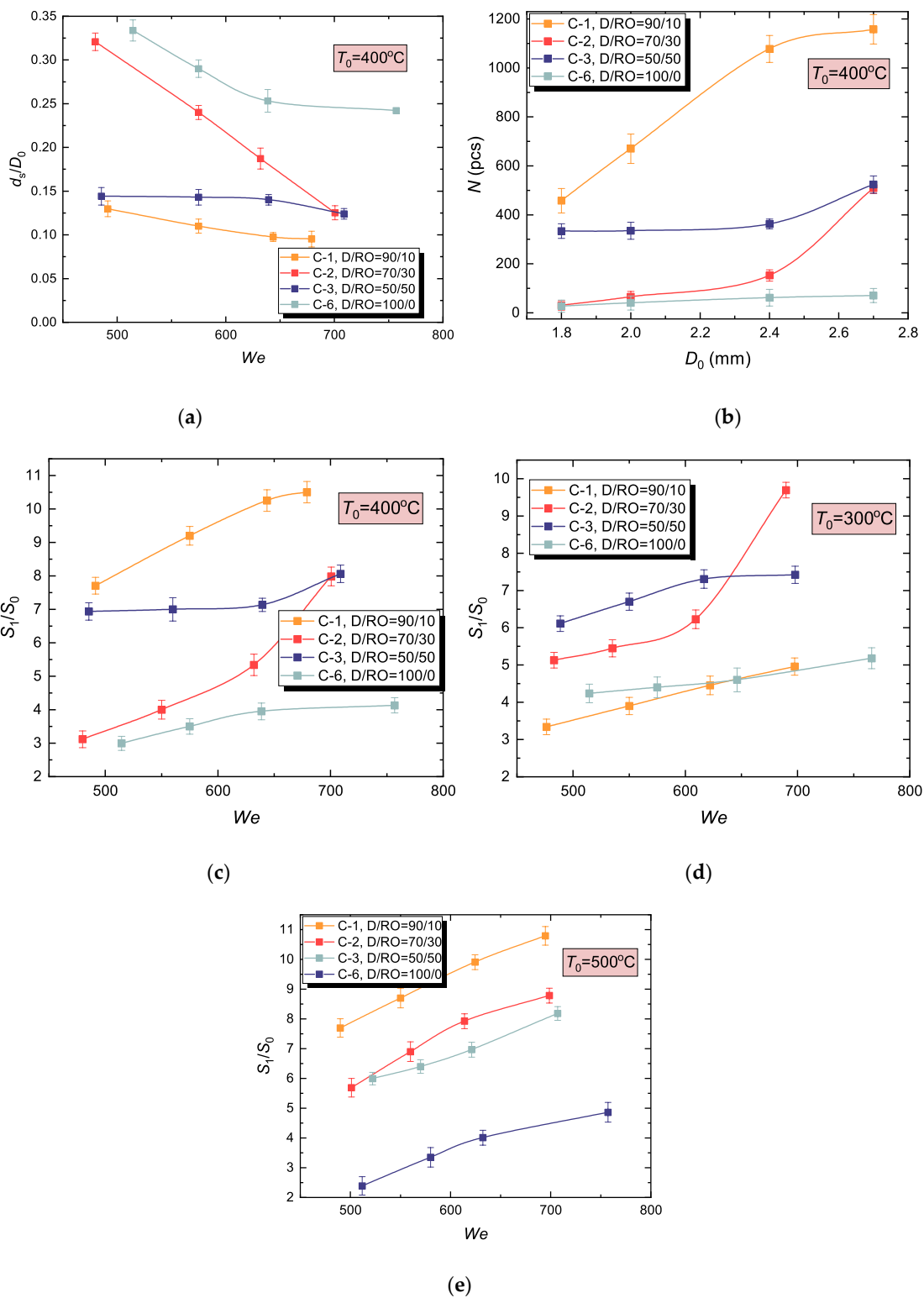


Figure 8. Effect of FAME of rapeseed oil (RO) added to the hydrocarbon component of micro-emulsion in different volume fractions on (a) mean diameter of child droplets generated by hydrodynamic breakup, (b) their amount, and (c–e) fuel evaporation surface area; (a–c) $T_0 = 400\text{ }^\circ\text{C}$, (d) $T_0 = 300\text{ }^\circ\text{C}$, (e) $T_0 = 500\text{ }^\circ\text{C}$.

The effect of inertial forces, viscosity, and surface tension results in different outcomes of the impact characterized by specific thermodynamic processes. The analysis of Figure 8 shows that a threshold We was observed for almost every liquid. When S_1/S_0 exceeds this threshold, its values do not change much, i.e., the curves tend to asymptotic values. These trends were observed at various temperatures and for various droplet component compositions. By considering them, we will be able to optimize the secondary atomization due to the wall impact. Indeed, it is unreasonable to increase the impact velocity or initial drop size trying to provide $We > 300$, if the child to parent droplet size ratio (and, correspondingly, S_1/S_0) will only change by 15–20%. More rational parameters should be chosen in this case.

Again, composition C-1 demonstrated the highest integral characteristics of hydrodynamic breakup with an increase in T_0 (Figure 8e). At $T_0 = 300\text{ }^\circ\text{C}$, adding the minimum amount of biodiesel had no perceptible effect on S_1/S_0 (Figure 8d). The results in Figure 8c–e indicate the following:

- (1) Viscosity decrease due to adding a minimum amount of biodiesel provides a several-fold increase in the number of fine child droplets.
- (2) Wall surface temperature should be taken into an account when analyzing the integral characteristics of the hydrodynamic breakup of WiDME and WiBDME drops.
- (3) Fuel micro-emulsion drops with FAME of rapeseed oil break up into more child droplets with a smaller mean diameter, intensifying the air-fuel mixture preparation in the combustion chamber.

The effect of rheological properties of a fuel composition on WiDME and WiBDME droplet spreading diameter versus time (Figure 9) was studied experimentally. First, it is important to emphasize several specific aspects of the interaction between WiDME and WiBDME droplets (see insets in Figure 9a). Having the lowest viscosity of all the examined compositions, C-5 droplets break up with the corona splash stage dominating at any temperature typical of the hydrodynamic breakup, i.e., $300\text{ }^\circ\text{C}$ (Figure 9a), $400\text{ }^\circ\text{C}$ (Figure 9b), and $500\text{ }^\circ\text{C}$ (Figure 9c). In the terms from [16], a rounded corona is formed. At the same time, C-6 droplets, having one of the highest viscosities, interact with the surface with distinctive fingering followed by finger breakup under the same temperature conditions (Figure 9a–c).

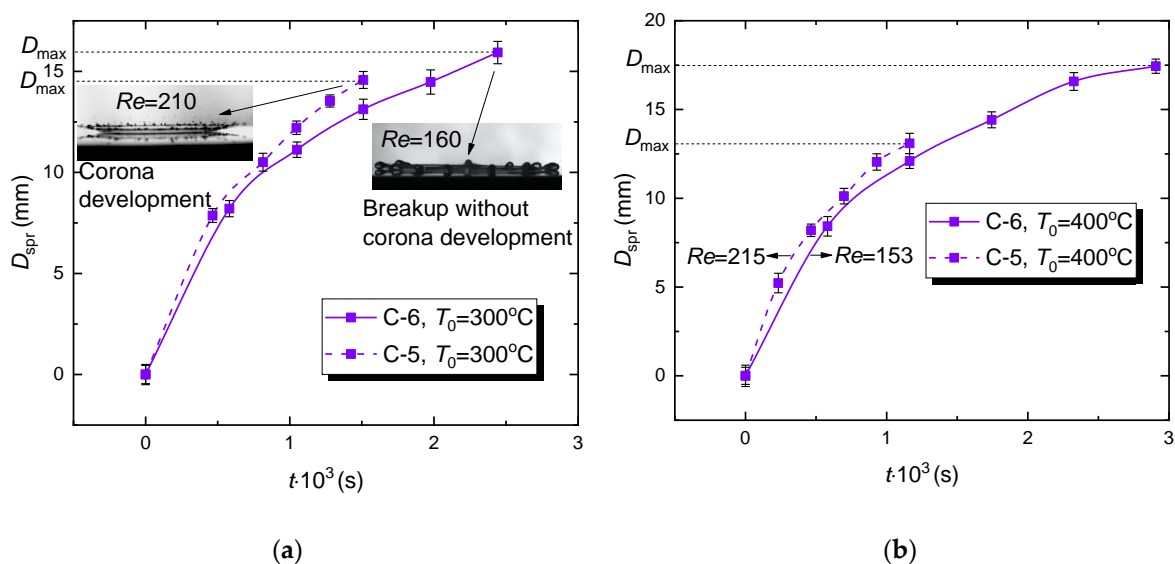
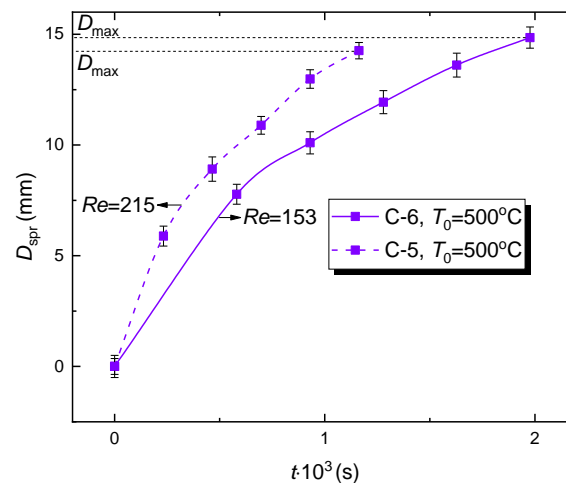


Figure 9. Cont.



(c)

Figure 9. Variation of the spreading diameter of WiDME (C-6) and WiBDME (C-5) droplets versus time at different surface temperatures: (a) $T_0 = 300\text{ °C}$, (b) $T_0 = 400\text{ °C}$, (c) $T_0 = 500\text{ °C}$; slight difference in Re with other factors being equal is caused by minimum deviation of the average parent drop diameter.

The main conclusions on how the rheological properties of fuel compositions affect the temporal variations of the WiDME (C-6) and WiBDME (C-5) droplet spreading diameters are as follows:

- (1) A considerable decrease in WiBDME viscosity promotes corona development when a droplet collides with a wall;
- (2) Due to a corona formation (corona splash), a WiBDME droplet breaks up faster than WiDME droplet in the same experimental conditions (Figure 9). During the corona development, a rim is highly unstable, promoting its quick disruption after the crown is formed;
- (3) Maximum spreading diameter D_{\max} of a WiBDME droplet is smaller than that of a WiDME droplet at all times (Figure 9);
- (4) Increased viscosity leads to fingering and impedes child droplet generation (Figure 9); thus, finger breakup generates fewer child droplets with a larger diameter (Figure 8);
- (5) The established features of droplet interaction after adding biodiesel resulting in a significant decrease in the sample viscosity adequately explain the difference in integral characteristics of the hydrodynamic breakup (Figure 8).

3.4. Effect of Emulsifier Concentration

In the examined three-component system, it is necessary to study the effect of emulsifier on droplet disintegration characteristics, since the volume concentration of this component can be as high as 30–40% [23]. Therefore, the impact of this component on micro-emulsion rheology can be quite substantial. To study this factor, we used C-3 and C-5 compositions with volume concentrations of 20 vol.% and 10.45 vol.%. All other composition properties were identical. Evidently, with lower emulsifier concentrations, a micro-emulsion drop disintegrates on impact into smaller fragments (Figure 10a). At the same time, the C-5 composition (Table 3) has one of the lowest viscosities among the examined micro-emulsions. Therefore, since emulsifier concentration growth increases the composition viscosity (Table 3), an increase in the proportion of emulsifier in the fuel mixture has an overall negative effect on the quantitative integral characteristics of disintegration (Figure 10b). Notably, parameters d_s/D_0 and S_1/S_0 of every examined composition (Figure 10) at maximum We converge to a single point for each substrate surface temperature. This can be explained by a much more substantial effect of inertial forces than substrate surface temperature T_0 on disintegration characteristics.

Figure 10 clearly shows that even high-viscosity droplets rapidly break up into a mist of child droplets at $We > 600$. The growth of S_1/S_0 can reach 5–13 times. This result describes certain threshold conditions for the secondary atomization of high-viscosity fuel at various wall temperatures.

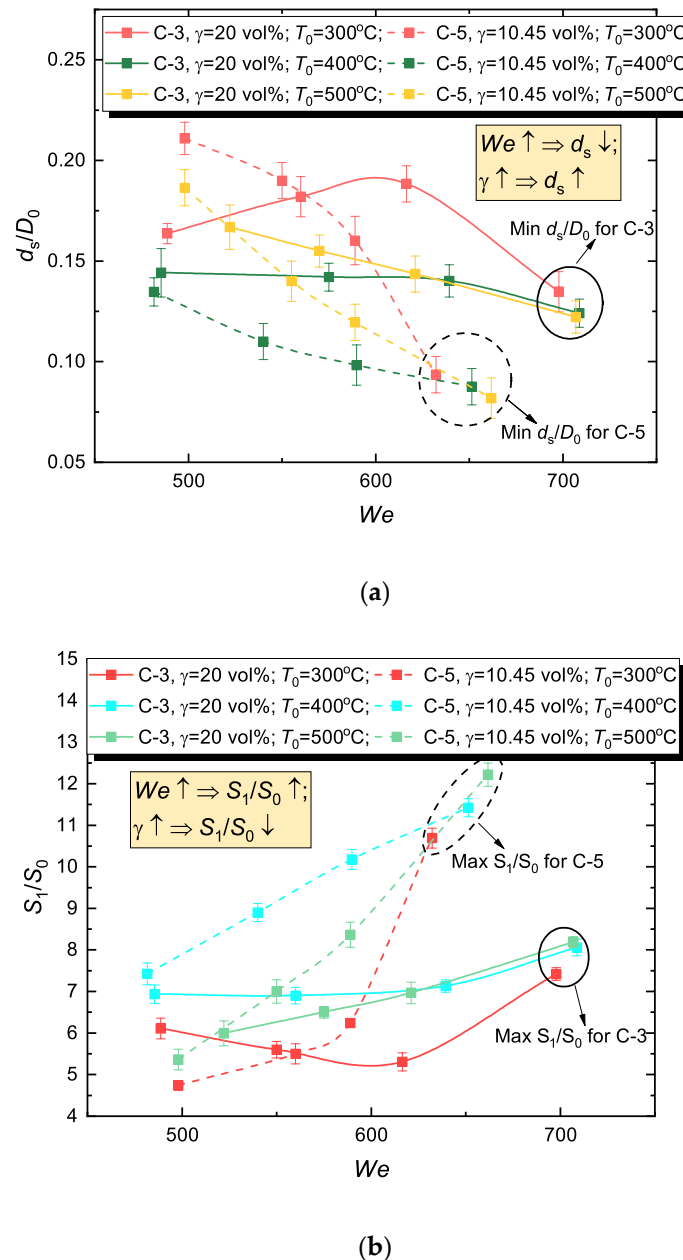
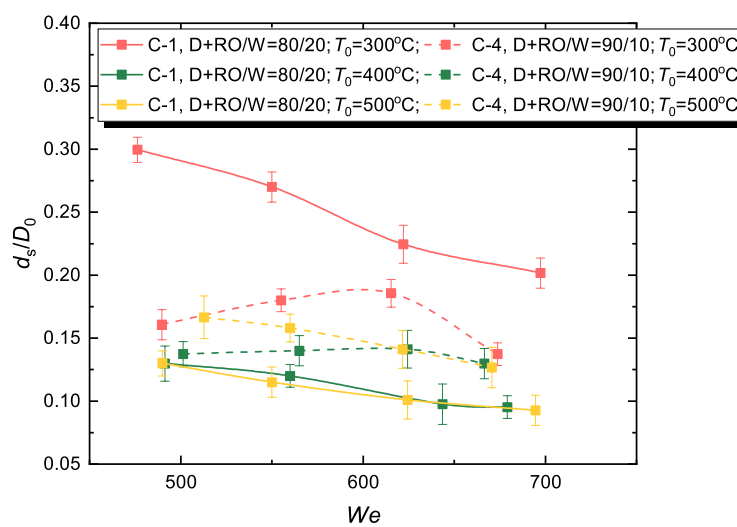


Figure 10. Effect of emulsifier concentration in WiBDME (C-3 and C-5) on hydrodynamic disintegration characteristics of corresponding fuel droplets (mean child droplet diameter (a) and evaporation surface area (b) at various surface temperatures).

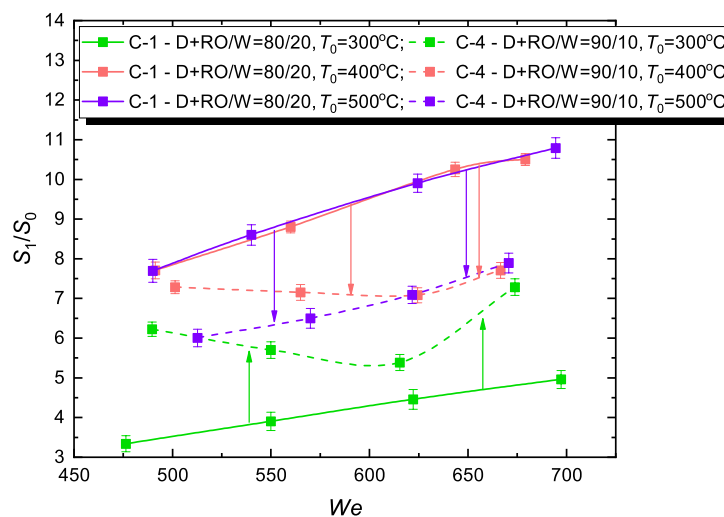
3.5. Effect of Water Concentration in Fuel Composition

It is also important to estimate the effect of changes in the water proportion in fuel micro-emulsions on the characteristics under study. For that we studied the interaction of a composition with a D+FAME/W ratio of 80/20 (16 vol.% water concentration) and 90/10 (8 vol.% water concentration) with a substrate heated to 300–500 °C (Figure 11). For D+FAME/W = 80/20, the mean diameter variation of the secondary fragment can exceed 50%, but with a lower proportion of water (D+FAME/W = 90/10), the variation becomes comparable to the measurement error (15–20%). Given that the two studied

WiBDME parameters are close (Table 3), the result can be explained by the factor of temperature. It means that a considerable amount of water in a WiBDME droplet will promote the film-boiling-induced disintegration [16] with abundant heat supply to a spreading drop lamella. This will be accompanied by rapid phase transformation and consecutive breakup (Figures 5a and 6a). This process is rather inconsistent in general and the droplets generated as a result significantly vary in size (Figure 11a). With $D+FAME/W = 90/10$ (i.e., C-4 composition is close to a diesel/biodiesel blend), the drops break up into almost identical fragments for any studied temperature T_0 (Figure 11a). This has a negative impact on the integral characteristic (Figure 11b): it hardly varies with the growing T_0 and remains moderate (about 5.5–7.5) with an increase in We unlike S_1/S_0 of C-1 droplets whose surface area increased more than 10 times after disintegration (Figure 11b). Therefore, the higher the water proportion in the micro-emulsion, the greater the variation in the size of resulting fragments (Figure 11a), and, correspondingly, integral quantitative characteristics (Figure 11b).



(a)



(b)

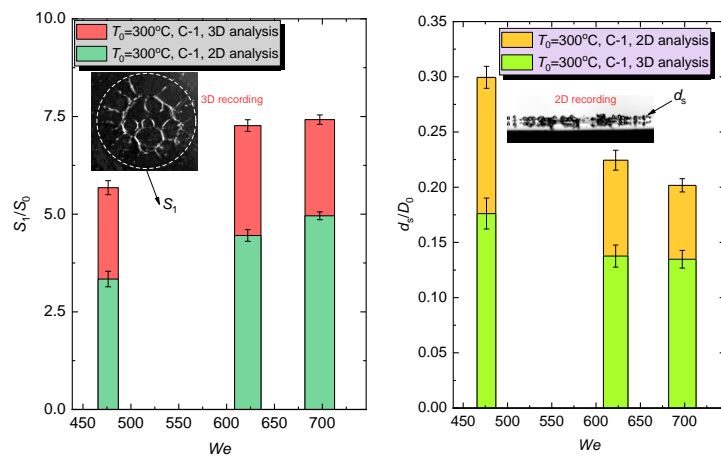
Figure 11. Effect of water concentration in WiBDME (C-1 and C-4) on hydrodynamic disintegration characteristics of corresponding fuel droplets (mean diameter of child droplets (a) and fuel evaporation surface area (b) at various surface temperatures).

The experimental curve trends in Figures 7, 8, 10 and 11 are similar in terms of the mean diameter of child droplets and variation of the liquid evaporation surface area.

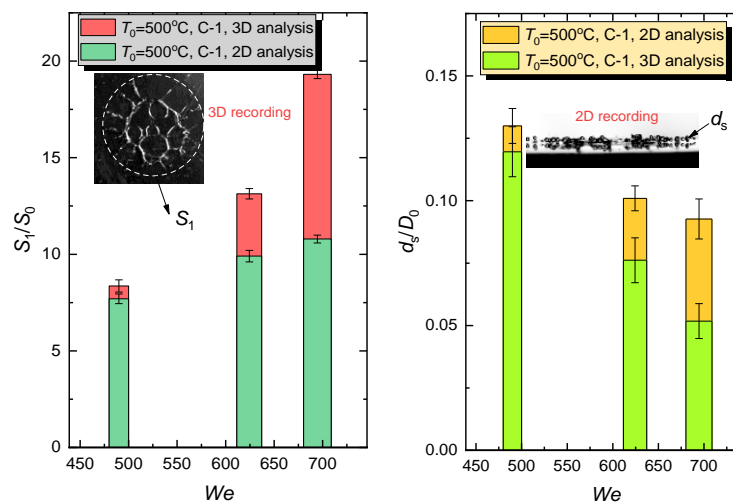
The effect of water fraction on child droplet generation is determinative for some of the secondary atomization techniques, in particular, for droplets colliding with each other or due to thermal micro-explosive breakup. It is shown in [36] that micro-explosive breakup response time is minimal for water proportions of 3 vol.% or 97 vol.%, i.e., for very low or very high values. This is due to high heat capacity and high vaporization heat of water. These two parameters are several-fold higher than those of any liquid fuel. As a result, an increase in the water proportion also increases the overall heat capacity and heat consumption in evaporation. This also prolongs droplet heating to the breakup point. The lower the proportion of water, the faster its local overheating is achieved, which is sufficient for disintegration. The surface tension of the liquid combustible component is much lower than that of water. So, even when water was overheated locally, the parent droplet rapidly broke up. Under heating, the surface tension, viscosity, and density of the combustible and non-combustible components went down. Therefore, a fine aerosol formed due to micro-explosion was not unexpected. However, our experiments [36] showed that large concentrations of water (up to 97 vol.%) in heterogeneous droplets also provide a micro-explosive breakup. Most likely, this happens because such a small volume of the liquid combustible component heats up very fast. This leads to the overheating of the inter-component interface above the water boiling temperature. Therefore, bubbles emerge at this interface but they do not grow as rapidly as in the experiments with more than 97 vol.% of the combustible component. Therefore, with high water concentrations in the droplets, micro-explosions occurred after a longer heating time and produced fewer child droplets. When the concentrations of the combustible and non-combustible components were equal in a droplet, both mechanisms affected the overheating of the interface above the water boiling temperature. In this case, the heating times were longer than in the experiments from [36] with 97 vol.% of the combustible component or 97 vol.% of the non-combustible component. However, if droplets contained several combustible components, the micro-explosion was affected not only by the thermophysical properties and vaporization heat but also by the differences in the surface tension and viscosity. The lower these parameters, the faster the parent droplets break up and the more child droplets are produced. The more combustible components are present in a heterogeneous droplet, the more complex are the functions of heating times to micro-explosion versus volume concentration of the combustible or non-combustible components. For droplets with several combustible components, the shortest heating times to micro-explosion may be provided by several combinations of relative volume concentrations [36]. Therefore, the results of [36] serve as another evidence to the main hypothesis that the local droplet overheating (i.e., heating of a small amount of liquid to the water boiling point) is enough for intense micro-explosive breakup. In this case, even fuel droplets with a high water concentration can break up intensely after colliding with a heated wall. The data of from [36] and results of this study enable the prediction of threshold requirements for extensive secondary atomization of droplets with various water concentrations.

3.6. Comparing the Results of Disintegration Characteristics Analysis by 2D and 3D Recording

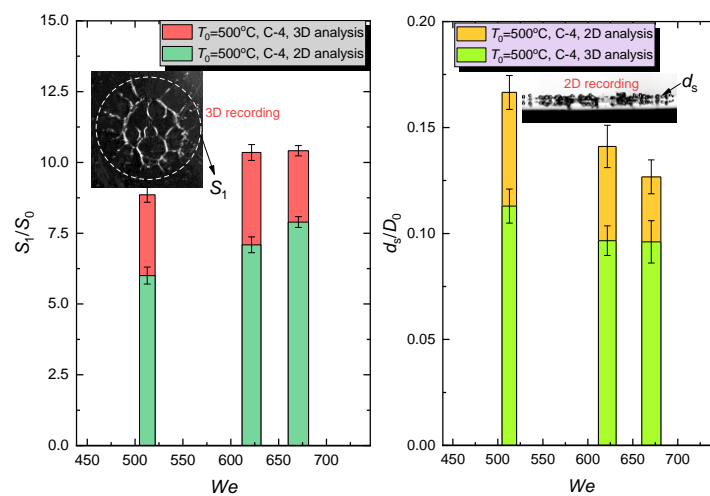
One of the objectives of this research was to establish the difference in the integral characteristics of hydrodynamic disintegration when using 3D recording and 2D recording of the outcome. Similar to the tests, the results of which are presented in Sections 3.1–3.5, we conducted experiments with three-dimensional recording of quantitative parameters and compared several d_s/D_0 and S_1/S_0 for the two measurement techniques (Figure 12).



(a)



(b)



(c)

Figure 12. Comparison of integral characteristics of hydrodynamic disintegration for 2D and 3D recording: (a) C-1, $T_0 = 300^\circ\text{C}$; (b) C-1, $T_0 = 500^\circ\text{C}$; (c) C-4, $T_0 = 500^\circ\text{C}$.

For the three-dimensional recording, the parameter d_s/D_0 was on average 24.5% lower at all times (Figure 12); the parameter S_1/S_0 was on average 28.5% higher. The difference is largely explained by the difficulty in the evaluation of smaller-diameter secondary fragments during the 2D recording, because their images were overlapped by larger droplets in the measurement area. This resulted in overestimated d_s/D_0 and correspondingly decreased S_1/S_0 . In general, the hydrodynamic disintegration characteristics can be evaluated using simpler and less laborious 2D recording technique, but only with the use of an adjustment coefficient. The overall trends of d_s/D_0 decrease and S_1/S_0 growth with the increasing We remained unchanged for both 3D and 2D recording techniques (Figure 12).

The experiments in [31] showed that the preliminary heating of fuel droplets may increase the effect of two factors. The first one is a decrease in the surface tension and viscosity, increasing the amount of fine child droplets after primary and secondary atomization. The second one is the increased evaporation rate of a droplet and a vapor buffer layer forming around it, acting as thermal insulation by deterring the heat flux to the droplet surface. This vapor buffer layer also decreases the relative impact velocity when heated droplets interact with each other. This factor promotes the interaction of droplets in the rebound regime, i.e., preserving their initial size. This way, the increased droplet vaporization can hinder its disintegration, despite the decrease in the surface tension and viscosity. The two factors have an opposing effect on the characteristics of the child droplets. It was shown in [31] that for initial droplet temperatures of 20 °C and 80 °C, these characteristics may vary from 15% to 50%. Thus, we can formulate a hypothesis that the experimental results of the current research are the upper estimate of S_1/S_0 achievable in a combustion chamber, because fuel droplets will be heated up to a high temperature prior to their collision with a wall. As a result, the formation of a buffer vapor layer around the droplets is of high probability.

For further research, it is proposed that we should study the kinematic stability and rheology of the biofuel microemulsions under a wide range of ambient temperatures, as well as to explore the effects of various bio-additives (e.g., fatty acid methyl ester of sunflower oil) on the drop impact processes, and to proceed with the tests on the primary and secondary atomization of the fuel microemulsion flows. The latter is difficult to implement without the results of the tests with impinging single drops.

4. Conclusions

The experiments have established that the regimes and outcomes of the interaction between diesel or biodiesel fuel micro-emulsion droplets and a heated wall have critical differences from the corresponding parameters known for other liquids. For example, by adding up to 50% of vegetable additive to the carbohydrate component of a micro-emulsion and decreasing the emulsifier concentration down to 10.45 vol. %, one can achieve a corona splash drop disintegration regime. Two- and three-dimensional plots were built for the main parameters of the secondary atomization of liquid droplets (d_s/D_0 , S_1/S_0) colliding with a heated wall for various water concentrations in the micro-emulsion (8–16 vol. %), droplet heating temperatures (300–500 °C), dimensions (1.8–2.8 mm), velocities (3–4 m/s) and emulsifier concentrations (10.45 vol. % and 20 vol. %). The rheological properties of the examined compositions were measured and accounted for when analyzing the experimental results. For prospective micro-emulsion compositions, it is possible to achieve $S_1/S_0 = 19$ (maximum for the 3D recording) and $d_s/D_0 < 0.1$. We established the determinative effect of the substrate temperature and water proportion in the micro-emulsion composition on the droplet-wall interaction regime and outcome. The temperature growth in the range from 300 °C to 500 °C leads to droplet breakup scenarios in different heat exchange regimes. This in general promotes a distinct variation in the integral quantitative characteristics of hydrodynamically disintegrating biodiesel micro-emulsion fuel droplets. Increasing the water proportion from 8 vol. % up to 16 vol. % changes the mean diameter of a child droplet at 300–500 °C by more than 50%. In this case, the overall surface area of the child droplets also increases more than tenfold. When comparing the integral characteristics of hydrodynamically disintegrating biodiesel micro-emulsion fuel droplets obtained via 2D and 3D recording, the latter method gave on average 24.5% lower d_s/D_0 and 28.5% higher S_1/S_0 . With this in

mind, 2D recording technique can be used for the experiments as a simpler and less laborious method, but with the introduction of an adjustment coefficient to account for the dimensional distribution of the generated child droplets.

Author Contributions: Investigation, A.E.A. and N.A.K.; Writing—original draft, M.V.P.; Writing—review & editing, V.A.Y. All authors have read and agreed to the published version of the manuscript.

Funding: This research was funded by [Russian Science Foundation] grant number [18-73-00083].

Conflicts of Interest: The authors declare no conflict of interest.

References

1. Tang, C.; Qin, M.; Weng, X.; Zhang, X.; Zhang, P.; Li, J.; Huang, Z. Dynamics of droplet impact on solid surface with different roughness. *Int. J. Multiph. Flow* **2017**, *96*, 56–69. [[CrossRef](#)]
2. Matsui, Y.; Sugihara, K. Sources of Hydrocarbon Emissions from a Small Direct Injection Diesel Engine. In Proceedings of the SAE International Off-Highway and Powerplant Congress and Exposition, Milwaukee, WI, USA, 14–17 September 1987.
3. Chou, T.; Patterson, D.J. In-cylinder measurement of mixture maldistribution in a L-head engine. *Combust. Flame* **1995**, *101*, 45–57. [[CrossRef](#)]
4. Kalghatgi, G.T.; Bradley, D. Pre-ignition and ‘super-knock’ in turbo-charged spark-ignition engines. *Int. J. Engine Res.* **2012**, *13*, 399–414. [[CrossRef](#)]
5. Bhat, M.; Sakthikumar, R.; Sivakumar, D. Fuel drop impact on heated solid surface in film evaporation regime. *Chem. Eng. Sci.* **2019**, *202*, 95–104. [[CrossRef](#)]
6. Chen, R.-H.; Chiu, S.-L.; Lin, T.-H. On the collision behaviors of a diesel drop impinging on a hot surface. *Exp. Therm. Fluid Sci.* **2007**, *32*, 587–595. [[CrossRef](#)]
7. Wachters, L.H.J.; Westerling, N.A.J. The heat transfer from a hot wall to impinging water drops in the spheroidal state. *Chem. Eng. Sci.* **1966**, *21*, 1047–1056. [[CrossRef](#)]
8. Chandra, S.; Avedisian, C.T. On the collision of a droplet with a solid surface. *Proc. R. Soc. Lond. Ser. A Math. Phys. Sci.* **1991**, *432*, 13–41. [[CrossRef](#)]
9. Karl, A.; Frohn, A. Experimental investigation of interaction processes between droplets and hot walls. *Phys. Fluids* **2000**, *12*, 785–796. [[CrossRef](#)]
10. Kompinsky, E.; Dolan, G.; Sher, E. Experimental study on the dynamics of binary fuel droplet impacts on a heated surface. *Chem. Eng. Sci.* **2013**, *98*, 186–194. [[CrossRef](#)]
11. Sen, S.; Vaikuntanathan, V.; Sivakumar, D. Impact dynamics of alternative jet fuel drops on heated stainless steel surface. *Int. J. Therm. Sci.* **2017**, *121*, 99–110. [[CrossRef](#)]
12. Sen, S.; Vaikuntanathan, V.; Sivakumar, D. Experimental investigation of biofuel drop impact on stainless steel surface. *Exp. Therm. Fluid Sci.* **2014**, *54*, 38–46. [[CrossRef](#)]
13. Bai, C.; Gosman, A.D. Development of Methodology for Spray Impingement Simulation. *SAE Int.* **1995**, *104*, 550–568.
14. Bai, C.X.; Rusche, H.; Gosman, A.D. Modeling of Gasoline Spray Impingement. *At. Sprays* **2004**, *12*, 1–28. [[CrossRef](#)]
15. Naber, J.D.; Reitz, R.D. Modeling Engine Spray/Wall Impingement. *SAE Int.* **1988**, *97*, 118–140.
16. Moreira, A.L.N.; Moita, A.S.; Panão, M.R. Advances and challenges in explaining fuel spray impingement: How much of single droplet impact research is useful? *Prog. Energy Combust. Sci.* **2010**, *36*, 554–580. [[CrossRef](#)]
17. Lif, A.; Stark, M.; Nydén, M.; Holmberg, K. Fuel emulsions and microemulsions based on Fischer–Tropsch diesel. *Colloids Surf. A Physicochem. Eng. Asp.* **2010**, *354*, 91–98. [[CrossRef](#)]
18. Leng, L.; Yuan, X.; Zeng, G.; Wang, H.; Huang, H.; Chen, X. The comparison of oxidative thermokinetics between emulsion and microemulsion diesel fuel. *Energy Convers. Manag.* **2015**, *101*, 364–370. [[CrossRef](#)]
19. Ding, Z.; Hao, A.; Wang, Z. Water-in-gasoline microemulsions stabilized by polyglycerol esters. *Fuel* **2007**, *86*, 597–602. [[CrossRef](#)]
20. Mukherjee, P.; Padhan, S.K.; Dash, S.; Patel, S.; Mohapatra, P.K.; Mishra, B.K. Effect of temperature on pseudoternary system Tween-80–butanol–hexane–water. *J. Colloid Interface Sci.* **2011**, *355*, 157–163. [[CrossRef](#)]

21. Najjar, R.; Heidari, S. Modified diesel prepared by stabilization of water as nanodroplets in diesel/colza oil blend: Study of phase behavior and affecting parameters. *Fuel* **2018**, *214*, 497–504. [[CrossRef](#)]
22. Acharya, B.; Guru, P.S.; Dash, S. Tween-80–n-Butanol–Diesel–Water Microemulsion System—A Class of Alternative Diesel Fuel. *J. Dispers. Sci. Technol.* **2014**, *35*, 1492–1501. [[CrossRef](#)]
23. Ashihmin, A.; Piskunov, M.; Roisman, I.; Yanovsky, V. Thermal stability control of the water-in-diesel microemulsion fuel produced by using a nonionic surfactant combined with aliphatic alcohols. *J. Dispers. Sci. Technol.* **2019**, *0*, 1–8. [[CrossRef](#)]
24. McClements, D.J. Nanoemulsions versus microemulsions: Terminology, differences, and similarities. *Soft Matter* **2012**, *8*, 1719–1729. [[CrossRef](#)]
25. Cen, C.; Wu, H.; Lee, C.; Liu, F.; Li, Y. Experimental investigation on the characteristic of jet break-up for butanol droplet impacting onto a heated surface in the film boiling regime. *Int. J. Heat Mass Transf.* **2018**, *123*, 129–136. [[CrossRef](#)]
26. Cen, C.; Wu, H.; Lee, C.; Fan, L.; Liu, F. Experimental investigation on the sputtering and micro-explosion of emulsion fuel droplets during impact on a heated surface. *Int. J. Heat Mass Transf.* **2019**, *132*, 130–137. [[CrossRef](#)]
27. Börnhorst, M.; Deutschmann, O. Single droplet impingement of urea water solution on a heated substrate. *Int. J. Heat Fluid Flow* **2018**, *69*, 55–61. [[CrossRef](#)]
28. Breitenbach, J.; Kissing, J.; Roisman, I.V.; Tropea, C. Characterization of secondary droplets during thermal atomization regime. *Exp. Therm. Fluid Sci.* **2018**, *98*, 516–522. [[CrossRef](#)]
29. Roisman, I.V.; Breitenbach, J.; Tropea, C. Thermal atomisation of a liquid drop after impact onto a hot substrate. *J. Fluid Mech.* **2018**, *842*, 87–101. [[CrossRef](#)]
30. Antonov, D.V.; Vysokomornaya, O.V.; Piskunov, M.V.; Shlegel, N.E. Analysis of statistical data on drop collisions in an aerosol flow during experiments. *EPJ Web Conf.* **2019**, *196*. [[CrossRef](#)]
31. Solomatin, Y.; Shlegel, N.E.; Strizhak, P.A. Atomization of promising multicomponent fuel droplets by their collisions. *Fuel* **2019**, *255*. [[CrossRef](#)]
32. Ashikhmin, A.E.; Piskunov, M.V.; Yanovskii, V.A. Hydrodynamic Regimes of Interaction between a Droplet of Water-in-Diesel Microemulsion and a Horizontal Heated Wall. *Tech. Phys. Lett.* **2019**, *45*, 544–548. [[CrossRef](#)]
33. Bernardin, J.D.; Stebbins, C.J.; Mudawar, I. Mapping of impact and heat transfer regimes of water drops impinging on a polished surface. *Int. J. Heat Mass Transf.* **1997**, *40*, 247–267. [[CrossRef](#)]
34. Bertola, V. An impact regime map for water drops impacting on heated surfaces. *Int. J. Heat Mass Transf.* **2015**, *85*, 430–437. [[CrossRef](#)]
35. Volkov, R.S.; Kuznetsov, G.V.; Strizhak, P.A. Water droplet deformation in gas stream: Impact of temperature difference between liquid and gas. *Int. J. Heat Mass Transf.* **2015**, *85*, 1–11. [[CrossRef](#)]
36. Antonov, D.V.; Strizhak, P.A. Heating, evaporation, fragmentation, and breakup of multi-component liquid droplets when heated in air flow. *Chem. Eng. Res. Des.* **2019**, *146*, 22–35. [[CrossRef](#)]

